Title

CX3CR1 ablation ameliorates motor and respiratory dysfunctions and improves survival of a Rett syndrome mouse model

Authors

Horiuchi, Makoto
Smith, Lucas
Maezawa, Izumi
et al.

Publication Date

2017-02-01

DOI

10.1016/j.bbi.2016.02.014

Peer reviewed

HHS Public Access

Author manuscript

Brain Behav Immun. Author manuscript; available in PMC 2017 July 27.

Published in final edited form as:

Brain Behav Immun. 2017 February ; 60: 106–116. doi:10.1016/j.bbi.2016.02.014.

CX_3CR1 ablation ameliorates motor and respiratory dysfunctions and improves survival of a Rett syndrome mouse model

Makoto Horiuchi[a], **Lucas Smith**[a], **Izumi Maezawa**[a,b], and **Lee-Way Jin**[a,b,*]

[a]Department of Pathology and Laboratory Medicine, 2805 50th Street, UC Davis Medical Center, Sacramento, CA 95817, United States

[b]M.I.N.D. (Medical Investigation of Neurodevelopmental Disorders) Institute, 2805 50th Street, UC Davis Medical Center, Sacramento, CA 95817, United States

Abstract

Rett syndrome (RTT) is a neurodevelopmental disorder caused by loss-of-function mutations in the gene encoding MeCP2, an epigenetic modulator that binds the methyl CpG dinucleotide in target genes to regulate transcription. Previously we and others reported a role of microglia in the pathophysiology of RTT. Because microglia in the *Mecp2* knockout (*Mecp2KO*) mouse model of RTT over-produce neurotoxic mediators glutamate and reactive oxygen species, we hypothesize that blocking neuron–microglia interaction by ablation of CX_3CR1, a chemokine receptor expressed in microglia/myeloid cells mediating such interaction by pairing with its neuronal ligand CX_3CL1, would ameliorate the RTT-like phenotype in *Mecp2KO* mice. Here we report that CX_3CR1 ablation prolonged the lifespan of *Mecp2KO* mice from a median survival of 54.5–74 days, and significantly improved the body weight gain, symptomatic scores, major respiratory parameters, and motor coordination and performance. CX_3CR1 ablation rectified previously identified histological abnormalities in the *Mecp2KO* brain such as neuronal soma size in hippocampal CA2, and the number, soma size, and process complexity of microglia. Moreover, CX_3CR1 ablation enhanced the neurotrophic action of microglia in *Mecp2KO* mice by producing higher amount of insulin-like growth factor 1. Our data support a role of myeloid cells/microglia in RTT and suggest a novel therapeutic approach for RTT by targeting CX_3CR1 with specific antagonists or genetic downregulation.

Keywords

ett syndrome; MeCP2; Microglia; CX_3CR1

1. Introduction

Rett syndrome (RTT) is caused by loss-of-function mutations in the X-linked gene encoding the epigenetic regulator MeCP2. RTT is a prototype of postnatal neurodevelopmental disorders affecting synaptic plasticity, and shares common mechanisms with autism (Zoghbi, 2003). RTT primarily affects young girls (*Mecp2*−/+), who develop normally until six to 18

*Corresponding author at: Dept. of Pathology and Laboratory Medicine, University of California Davis Medical Center, Sacramento, CA 95817, United States. lwjin@ucdavis.edu (L.-W. Jin).

months of age, when they start to regress, showing deceleration of brain growth, loss of motor skills including purposeful hand movements, ataxia, loss of vocalization skills, loss of cognitive capability, autistic features, seizures, and respiratory dysfunction (Chahrour and Zoghbi, 2007).

The absence of MeCP2, which "reads" DNA methylation marks, blocks the effective recognition and execution of epigenetic codes, resulting in altered gene expression and cellular function (Chahrour et al., 2008). Although such biochemical function of MeCP2 is well delineated, the specific mutant-driven toxic mechanisms that initiate and promote progression of RTT remain unclear. Deletion of *Mecp2* in neuronal populations led to RTT-like pathology in mice (Chen et al., 2001; Chao et al., 2010), suggesting an initiating role of neuronal MeCP2 deficiency, although such neuron-driven phenotype was partial and mild. Interestingly, recovering wild-type (WT) *Mecp2* in astrocytes or microglia/myeloid cells in the *Mecp2* knockout (*Mecp2KO*) model of RTT arrested RTT-like pathology, suggesting that dysfunction of non-neuronal cells contributes to progression of disease (Lioy et al., 2011; Derecki et al., 2013; Cronk et al., 2015a). In contrast, neuronal re-expression of WT *Mecp2* in *Mecp2KO* mice failed to rescue RTT-like phenotype (Alvarez-Saavedra et al., 2007). Taken together, the RTT pathology appears to result from contributions from different cell types and may in large part depend on neuron-glia interactions.

Myeloid cells and brain resident microglia appear to play a significant role in RTT (Maezawa and Jin, 2010; Derecki et al., 2012; Cronk et al., 2015b; Jin et al., 2015). Remarkably, *Mecp2KO* mice, which usually die at 9–10 weeks, became almost normal and some lived to nearly one year after their brains were populated with WT peripherally-derived resident CNS macrophages by a bone-marrow transplant approach. When cranial irradiation was blocked to prevent microglial engraftment, disease was not arrested, suggesting that the effect mainly came from microglia (Derecki et al., 2012). Furthermore, phenotypic reversal was observed after re-expression of WT *Mecp2* selectively in myeloid cells/microglia, directed by *Lysm*- or *Cx3cr1*-driven cre (Derecki et al., 2012; Cronk et al., 2015b). However, this key set of results was not reproduced in a recent independent study (Wang et al., 2015). Thus, the contribution of myeloid cells/microglia remains unresolved.

To shed light on this controversy, we employed an alternative approach to test the pathological significance of myeloid cells/microglia in RTT. We ablated CX_3CR1 in *Mecp2KO* mice and determined the phenotypic consequences. CX_3CR1, a chemokine receptor expressed in myeloid cells/microglia during development and adulthood, mediates neuron–microglia interaction by pairing with its ligand CX_3CL1 expressed in neurons; this pairing is able to modulate microglia activation and neurotoxicity (Cardona et al., 2006; Limatola and Ransohoff, 2014; Zhan et al., 2014). Because microglia in *Mecp2KO* mice constitutively produce high levels of neurotoxic mediators such as glutamate and reactive oxygen species (Maezawa and Jin, 2010; Jin et al., 2015), we hypothesize that neuron–microglia interactions detrimentally affect neuronal and synaptic integrity in RTT. Ablation of CX_3CR1, therefore, would ameliorate the RTT-like phenotype in *Mecp2KO* mice. Here we report that CX_3CR1 ablation indeed improved several major aspects of RTT pathology, thus providing a fresh line of evidence to support a role of myeloid cells/microglia in RTT and suggest a therapeutic potential for CX_3CR1 antagonists.

2. Materials and methods

2.1. Animals

Mecp2$^{tm1.1Bird/+}$ mice, originally generated in Dr. Adrian Bird's laboratory (Guy et al., 2001), and mice with *Cx*$_3$*cr1*-EGFP targeted mutation (B6.129P-*Cx*$_3$*cr1*^{tm1Litt}/J) were obtained from the Jackson Laboratories (Bar Harbor, Maine). Both lines have been maintained in the C57BL/6 J genetic background (Jackson Laboratories). To generate mice with both *Mecp2* and *Cx*$_3$*cr1* deletion, female *Mecp2*$^{+/-}$ mice were first mated with male *Cx*$_3$*cr1*$^{-/-}$ mice to produce *Mecp2*$^{+/-}$–*Cx*$_3$*cr1*$^{+/-}$ females, which were then crossed with *Mecp2*$^{+/y}$–*Cx*$_3$*cr1*$^{+/-}$ males to produce littermates of male *WT* (*Mecp2*$^{+/y}$–*Cx*$_3$*cr1*$^{+/+}$) and *Mecp2KO* mice of three genotypes (*Mecp2*$^{-/y}$–*Cx*$_3$*cr1*$^{+/+}$, *Mecp2*$^{-/y}$–*Cx*$_3$*cr1*$^{+/-}$, and *Mecp2*$^{-/y}$–*Cx*$_3$*cr1*$^{-/-}$) for comparison. Additional male *Mecp2KO* (*Mecp2*$^{-/y}$–*Cx*$_3$*cr1*$^{+/+}$) mice were obtained from mating between female *Mecp2*$^{+/-}$ mice with male *WT Mecp2*$^{+/y}$ mice. We found no significant phenotypic and pathological differences between these two pools of male *Mecp2KO* mice and their data were combined. The Animals were housed in standard laboratory cages with unrestricted access to food and water, and maintained under 12 h light/dark cycles. The University of California Davis Institutional Animal Care and Use Committee approved all animal experiments.

2.2. Symptomatic scoring

Mice were weighed and examined twice a week. Neurological deficits of mice were examined for the five parameters (mobility, gait, hindlimb clasping, tremor, and general condition) as described by Guy et al. (2001). For mobility, each mouse was removed from the home cage and placed onto the center of a clean cage and scored as following – movement as well as *WT* mice (score = 0); reduced movement and extended freezing period compared to *WT* mice (score = 1); and complete loss of movement (score = 2). For gait, each mouse was placed onto a metal bench surface and scored as following – same to *WT* mice (score = 0); hindlimbs spread wider than *WT* mice (score = 1); and lack of full strides by hindlimbs resulting in drugging them (score = 2). For hindlimb clasping, each mouse was suspended by the tail and scored as following – both hindlimbs spreading outward as *WT* mice (score = 0); one hindlimb pulled into the body (score = 1); and both hindlimb pulled into the body or forming a widened bowl shape (score = 2). For tremor, each mouse was held in the palms of experimenter's hands for 1 min to feel their shake and scored as following – no tremor (score = 0); intermittent mild tremor (score = 1); continuous tremor or intermitted strong tremor (score = 2). For general condition, coat and eye conditions of each mouse were examined and scored as following – shiny coat, and clear and opened eyes (score = 0); ungroomed coat, or dull or squinty eyes (score = 1); ungroomed coat, and dull or squinty eyes (score = 2). A total score for each mouse/time point was obtained from adding individual scores from the four categories and was recorded as a single data point for statistical analysis.

2.3. Plethysmography

Respiration parameters in mice between 5 and 9 week-old were recorded using a whole-body plethysmogram (Emka technologies, Falls church, VA). Unrestrained and unanesthetized mice were placed in the plethysmograph chamber to which a constant inflow

of fresh air (0.8 L/min) was supplied. Mice were habituated to the chamber for 5 min prior to recording, and then recordings were performed for 30 min at room temperature. Pressure change in the chamber was detected by a differential pressure transducer. The signal from the transducer was amplified and converted to digital signal, which was further processed and stored by the iox software (Emka technologies) in real time. Apneas (expiratory time >1 s) and other respiratory parameters were recorded and calculated using the iox software.

2.4. Motor tests

All the following tests were performed during the light phase. Mice were allowed to acclimate for more than 30 min before each test.

2.4.1. Open-field test—General motor activity, willingness of exploration, and anxiety were examined by the open-field test (Stearns et al., 2007; Derecki et al., 2012; Garg et al., 2013). Each mouse was placed on the center of the monitoring cage (29.8 × 18.0 × 12.8 cm) and allowed to explore freely for 10 min. Mouse activity was monitored by SmartCage (AfaSci Research Laboratory, Redwood City, CA). The data was recorded and analyzed by Cage Center and Cage Score 2 softwares, respectively (AfaSci Research Laboratory) (Khroyan et al., 2012).

2.4.2. Rotarod test—Motor coordination and balance were examined on Rotamex-5 accelerating rotarod (Columbus Instruments, Columbus, OH) (Robinson et al., 2012). Each mouse was placed on the rotarod rotating constantly at 4 rpm. Then, rotarod was accelerated every 10 s with a 1.3 rpm increment. The latency to fall from the rotarod was recorded. Testing consisted of three trials per day for two consecutive days with intertrial intervals of 5 min.

2.4.3. Static rod test—Motor coordination and balance were also examined by the static rods tests (Deacon, 2013). A wooden dowel with 60 cm length and 5 mm cross-section diameter was fixed horizontally by a G-clamp to the bench. Ten cm from the end of the rod near the bench was marked to denote the finishing line. Each mouse was placed at the far end of the rod with back facing the finishing line. The time taken to orientate 180° towards the finishing line and to travel to the finishing line was recorded. Each mouse had two trials and the better performance was used as a single data point for analysis.

2.4.4. Horizontal bar test—Forelimb strength and coordination were accessed by the horizontal bars test (Deacon, 2013). A 38-cm long metal bar with 4 mm and 6 mm cross-section diameters was held 60 cm above the bench surface and fixed. The experimenter let a mouse grasp the bar at the center with its forepaws only. Latency time to fall was recorded, and each trial was scored on a five-point scale (falling between 1 and 5 s = 1; falling between 6 and 10 s = 2; falling between 11 and 20 s = 3; falling between 21 and 30 s = 4; and no falling over 30 s or escape to the end of the bar = 5). Each mouse had three trials. The cumulative score of a total of six trials for each mouse was used as a single data point for analysis.

2.4.5. Gait analysis by CatWalk test—Gait of unforced running mice was analyzed using the CatWalk XT device (Noldus Information Technology, Leesburg, VA) (Vrinten and Hamers, 2003). Each mouse was placed on a glass walkway of CatWalk XT and allowed to run across it in an unforced manner. The footprints were recorded by a high-speed video camera. The data obtained from at least 5 runs to traverse the walkway were recorded at one trial. The video recording was further analyzed by the CatWalk XT 10.5 software (Noldus Information Technology) to calculate the gait parameters.

2.5. Acute isolation of microglia from mouse brain

Microglia were acutely isolated from the brain of juvenile or adult mouse without culturing as we reported previously (Jin et al., 2015). Briefly, brains were dissociated enzymatically with Neural tissue dissociation kit (Miltenyi Biotec, San Diego, CA). Microglia were subsequently purified by the magnetic-activated cell sorting (MACS) using anti-CD11b magnetic beads (Miltenyi Biotec). The whole procedure took about 90 min. Acutely isolated microglia were over 94% pure based on flow cytometry assessments (Jin et al., 2015).

2.6. Quantitative polymerase chain reaction (qPCR)

Total RNA was extracted from acutely isolated microglia and tissue samples using RNeasy mini kit (Qiagen, Valencia, CA). RNA samples from acutely isolated microglia were reverse-transcribed and pre-amplified with Ovation PicoSL WTA System V2 kit (NuGen, San Carlos, CA). RNA samples from tissue were converted to cDNA using iScript Reverse Transcription Supermix (Bio-Rad, Hercules, CA), which were then subjected to real-time PCR using SsoFast Eva-Green Supermix (Bio-Rad). The following forward/reverse primer pairs were used: *Cx3cr1*, 5′-tgagtgactggcacttcctg-3′/5′-gttccaaaggccacaatgtg-3′; *Cx3cl1*, 5′-acaccccaactccagtgaac-3′/5′-aaagccaggagacacaagga-3′; *Cd11b*, 5′-aaggattcagcaagccagaa-3′/5′-ggagggatgagagtccacat-3′: *Igf1*, 5′-tggatgctcttcagttcgtg-3′/5′-cacaatgcctgtctgaggtg-3′. Relative cDNA levels for the target genes were analyzed by the $2^{-\Delta\Delta Ct}$ method using *Actb* as the internal control for normalization (Livak and Schmittgen, 2001).

2.7. IBA-1 immunohistochemistry

Mice were deeply anesthetized by 4% isoflurane and transcardially perfused with PBS followed by 4% paraformaldehyde in PBS. Tissue samples were further fixed over-night in 4% paraformaldehyde in PBS. After wash with PBS, tissue samples were infused with 15% sucrose in PBS followed by 30% sucrose in PBS. Twenty μm cryostat sections were rinsed with PBS, and incubated with blocking solution (5% fetal bovine serum, 0.4% triton-x 100 in PBS) for 1 h and then with the primary rabbit anti-IBA1 antibody (1:1000, Wako pure chemical industries, Osaka, Japan) in the blocking solution at 4 °C over-night. The sections were then washed with PBS, incubated with a goat anti-rabbit secondary antibody conjugated with Alexa-568 (1:500, Life technologies, Grand Island, NY) at room temperature for 1 h, washed with PBS, and mounted with Vectashield containing DAPI (Vector laboratories, Burlingame, CA).

2.8. Cresyl violet staining

After wash with PBS, tissue sections were incubated in 0.1% cresyl violet (Sigma-Aldrich, St. Louis, MO) for 15 min. Stained sections were mounted with permount (Thermo Fisher scientific, Waltham, MA) after dehydration with a series of 70%, 95%, and 100% ethanol and xylene.

2.9. Enzyme-linked Immunosorbent Assay (ELISA)

Cerebral cortices, hippocampi, striata, cerebellums, and brain stems were dissected fresh from mice after transcardial perfusion with PBS, and then snap frozen. Tissue samples were homogenized in lysis buffer (137 mM NaCl, 20 mM Tris-HCl pH 8.0, 1% igapel, 10% glycerol, proteinase inhibitor mix, phosphatase inhibitor mix), incubated on ice for 15 min, and centrifuged at 1,500 rpm for 10 min. The supernatants were directly used for the total IGF1 detection. For the free IGF1 detection, the supernatants were filtered through Amicon 30 K (Millipore, Billerica, MA) to remove IGF binding protein-bound IGF1 as previously described (Ueno et al., 2013). Concentrations of IGF1 were measured using the Quantikine sandwich ELISA kit (R & D systems, Minneapolis, MN).

2.10. Statistical analysis

Data are presented as mean ± SEM unless otherwise noted. For life span data, statistical significance was determined by Kaplan-Meier survival analysis. For repeatedly measured data, such as body weight, phenotype score, and the latency time in the Rotarod test, two-way repeated measures ANOVA followed by Holm-Sidak *post hoc* test was employed. For other sets of data, statistical significance was determined by one-way ANOVA followed by Holm-Sidak *post hoc* test. $p < 0.05$ was considered as statistically significant.

3. Results

3.1. CX_3CR1 ablation improves the life span, body weight, and symptomatic scores of Mecp2KO mice

We have used the *Mecp2*$^{tm1.1Bird/+}$ model (Guy et al., 2001), with which we have characterized microglial abnormalities (Maezawa and Jin, 2010; Jin et al., 2015) and for which the respiratory and motor phenotype has been well documented (Viemari et al., 2005; Abdala et al., 2010; Voituron and Hilaire, 2011). The male *Mecp2−/y* (*Mecp2KO*) have been widely used as a RTT model due to their early, robust, and consistent phenotype. They show onset of RTT-like symptoms at around five to six weeks of age. There follows a period of rapid regression resulting in reduced spontaneous movement, clumsy gait, irregular breathing, hindlimb clasping, tremors, and weight loss. These mice usually die before 10 weeks of age.

To examine the effect of CX_3CR1 ablation on the pathology of RTT, we compared male littermates of WT, *Mecp2KO–Cx*$_3$*-cr1*$^{+/+}$ (abbreviated as *Mecp2KO*), *Mecp2KO–Cx*$_3$*cr1*$^{-/+}$, and *Mecp2KO–Cx*$_3$*-cr1*$^{-/-}$ mice. Quantitative PCR showed that the Cx_3cr1 transcript in *Mecp2KO* mice was significantly reduced in most of the brain regions examined except for the cerebellum (Fig. 1a). However, when the Cx_3cr1 mRNA level in microglia acutely isolated from whole WT and *Mecp2KO* brains were compared, there was no difference (Fig.

1b). This set of results is consistent with previous findings that the number of microglia in the brain was decreased in *Mecp2KO* mice (Jin et al., 2015; Cronk et al., 2015b), and indicates that microglia in *Mecp2KO* mice expressed Cx_3cr1 at the same level as those in WT mice. The level of *Cx3cr1* transcript in the brain and microglia of *Mecp2KO–Cx3cr1*$^{-/+}$ mice was 40–50% of those in *Mecp2KO* mice and was negligible in *Mecp2KO–Cx3cr1*$^{-/-}$ mice, as expected (Fig. 1a and b). In contrast, the levels of microglial *Itgam* transcript (coding for CD11b) were not different between the four genotypes (Fig. 1c). Furthermore, because MeCP2 deletion *per se* did not reduce the expressions of CX_3CR1 (Fig. 1b) and CX_3CL1 (Fig. 1d), ablating CX_3CR1 in *Mecp2KO* mice is suitable to reveal the role of CX_3CR1 signaling in RTT pathology.

Fig. 2a illustrates that at 8 weeks, the body size of *Mecp2KO– Cx3cr1*$^{-/+}$ and *Mecp2KO–Cx3cr1*$^{-/-}$ mice was comparable to that of WT mice, while *Mecp2KO* had smaller body size. Fig. 2b shows that although at 4 weeks there were no differences in body weight between *Mecp2KO* with or without CX_3CR1 ablation, both *Mecp2KO–Cx3cr1*$^{-/+}$ and *Mecp2KO–Cx3cr1*$^{-/-}$ mice continued to gain weight, contrasting the persistent poor weight gain of *Mecp2KO–Cx3cr1*$^{+/+}$ mice (Guy et al., 2001). To monitor the specific RTT-like features, we used an established symptomatic scale that scores the mobility, gait, hindlimb clasping, tremor, breathing, and general condition, which semi-quantitatively records the increasing severity of RTT-like symptoms starting from 4 weeks (Guy et al., 2007). The *Mecp2KO–Cx3cr1*$^{-/+}$ and *Mecp2KO–Cx3cr1*$^{-/-}$ mice thrived better with lower symptomatic scores than their *Mecp2KO* littermates; the differences reached statistical significance at 5 and 6 weeks (Fig. 2c). Intriguingly, there were no significant body-size and symptomatic differences between *Mecp2KO–Cx3cr1*$^{-/+}$ and *Mecp2KO–Cx3cr1*$^{-/-}$ mice. This result suggests that CX_3CR1 ablation, even partial, delays the progression of RTT. Similarly, the progression to death was slowed by CX_3CR1 ablation, as life spans of both *Mecp2KO–Cx3cr1*$^{-/+}$ (median: 73 day) and *Mecp2KO–Cx3cr1*$^{-/-}$ (median: 74 day) mice were significantly longer than that of *Mecp2KO* mice (median: 54.5 day) (Fig. 2d). These results suggest a contribution of CX_3CR1 signaling to the early development of RTT-like symptoms and the premature death of *Mecp2KO* mice.

3.2. CX_3CR1 ablation improves the respiratory parameters of Mecp2KO mice

A major cause of morbidity and mortality in RTT is dysfunctional respiratory control, manifesting irregular breathing patterns and striking episodes of apnea (Katz et al., 2009). To examine the effect of CX_3CR1 ablation on respiratory parameters of *Mecp2KO* mice, littermates of the four genotypes were subjected to wholebody plethysmographic recording. *Mecp2KO* mice showed a significant increase in the incidence of apnea as reported previously (Viemari et al., 2005; Zanella et al., 2008; Abdala et al., 2010). The apnea counts were reduced to close to normal in *Mecp2KO–Cx3cr1*$^{-/+}$ and *Mecp2KO–Cx3cr1*$^{-/-}$ mice (Fig. 3a–c). The low incidence of apnea in *Mecp2KO–Cx3cr1*$^{-/+}$ and *Mecp2KO–Cx3cr1*$^{-/-}$ mice was also apparent after their median survival times (73 and 74 days, respectively, Fig. 3b), which could contribute to their extended life span. Detailed analyses of respiratory variables of over 5000 consecutive respiratory cycles from each recording revealed that *Mecp2KO* mice showed significantly prolonged inspiratory time (Ti) and expiratory time (Te), and significantly reduced peak inspiratory flow (PIF), peak expiratory flow (PEF), tidal

ventilation (TV), and breathing frequency compared toWT mice. Among these variables, PEF and TV were significantly improved in *Mecp2KO–Cx$_3$cr1$^{-/+}$* and *Mecp2KO–Cx$_3$cr1$^{-/-}$* mice (Fig. 3d). These results suggest that CX_3CR1 ablation improved the coordination among multiple neuronal activities governing the respiratory pattern.

3.3. CX_3CR1 ablation improves the motor performance of Mecp2KO mice

Poor motor control, reduced exploratory behavior, and anxiety are among other major disabilities of RTT patients and mice. In the open-field test, *Mecp2KO* mice at 5–6 weeks of age showed reduced counts of rear up, and this abnormality was significantly ameliorated in *Mecp2KO–Cx$_3$cr1$^{-/+}$* and *Mecp2KO–Cx$_3$cr1$^{-/-}$* mice, suggesting that CX_3CR1 ablation reversed the reduced exploratory behavior in *Mecp2KO* mice. However, CX_3CR1 ablation failed to increase the shortened center time observed in *Mecp2KO* mice, suggesting that it offers no effect in alleviating anxiety (Fig. 4a). Further tests on motor functions showed that CX_3CR1 ablation improved the “cadence” (number of step/unit time) in the CatWalk gait test, prolonged the latency to fall from the rotarod, and improved the performance of *Mecp2KO* mice in horizontal bar and static rod tests (Fig. 4b–e), suggesting enhanced motor coordination and limb strength.

3.4. CX_3CR1 ablation recovers neuronal or microglial morphology of Mecp2KO mice

We next examined if CX_3CR1 ablation affects neuronal and microglial morphology. *Mecp2KO* brains do not show apparent morphological abnormalities, except small neuronal soma size prominently in the hippocampal CA2 (Chen et al., 2001). CX_3CR1 ablation in *Mecp2KO* mice restored the CA2 neuronal soma size to near WT levels (Fig. 5).

Consistent with published data (Cronk et al., 2015b; Jin et al., 2015), *Mecp2KO* brains also showed less microglia with less apparent processes compared to WT, demonstrated by IBA-1 immuno-labeling. CX_3CR1 ablation in *Mecp2KO* mice increased IBA-1-immunoreactive areas in the cerebral cortex, hippocampus, and striatum to near WT levels (Fig. 6a). In the striatum, for example, the number of microglia, the size of microglial soma, and the degree of ramification were all increased to WT levels, which could contribute to the improvement in motor functions (Fig. 6b–d).

3.5. CX_3CR1 ablation increases the expression of insulin-like growth factor 1 (IGF1) in Mecp2KO mice

Several microglia-related mechanisms modulated by the CX_3CL1–CX_3CR1 axis have been reported (Limatola and Ransohoff, 2014). Among them, keenly relevant to RTT is the ability of CX_3CR1 to regulate microglial IGF1 production. Microglia were shown to be an important source of IGF1, which exerts trophic support to certain groups of postnatal neurons through the IGF1 receptor and PI3 K-AKT pathway (Ueno et al., 2013). IGF1 deficiency was shown in *Mecp2KO* mice; treatment with recombinant human IGF1 was shown to prolong the lifespan and ameliorate RTT-like symptoms in *Mecp2KO* mice (Castro et al., 2014), not unlike the effects of CX_3CR1 ablation. We therefore hypothesized that CX_3CR1 ablation may upregulate IGF1 production by *Mecp2KO* microglia to boost the microglial neurotrophic function. We found that microglia in *Mecp2KO* mice had reduced levels of *Igf1* mRNA, which, after CX_3CR1 ablation, was significantly increased even above

the WT level (Fig. 7a). Concordantly, the levels of total IGF1 protein in *Mecp2KO* brains were quite low compared to WT, but were increased ~3-fold with CX_3CR1 ablation (Fig. 7b). We further measured the levels of IGF1 in the flow-through of the Amicon ultracentrifugal filter with a 30-KDa molecular mass cut-off, which represents free IGF1 (about 7 KDa in molecular weight) not bound to the regulatory IGF-binding proteins (IGFBPs), which may have distinct ligand avidities (Ueno et al., 2013). We found that the levels of free IGF-1 was also significantly reduced in the *Mecp2KO* brains compared with the WT brains, and the reduction was restored in *Mecp2KO–Cx3cr1*$^{-/-}$ mice but not in *Mecp2KO–Cx3cr1*$^{-/+}$ mice (Fig. 7c).

4. Discussion

The pathological role of microglia/myeloid cells in RTT remains controversial with recent conflicting *in vivo* results using mouse models (Derecki et al., 2012; Cronk et al., 2015b; Wang et al., 2015). Here, the observed influences of CX_3CR1, a key cytokine receptor in microglia/myeloid cells, on RTT-like presentations in mice provide an independent line of evidence clearly supporting a role of microglia/myeloid cells in RTT. Further studies are required to elucidate the roles of peripheral immune cells expressing CX_3CR1 such as neutrophils, monocytes, and T cells, which would also be affected by systemic CX_3CR1 ablation. Particularly, intestinal macrophages highly expressing CX_3CR1 could be interesting as the interplay between intestinal microbiota and the brain development has been suggested (Niess et al., 2005; Collins et al., 2012). However, the fact that in the brain CX_3CR1 was localized to microglia and CX_3CL1 to neurons (Harrison et al., 1998), and the repeated demonstrations that CX_3CL1/CX_3CR1-mediated neuron–microglia interaction modulates basic physiological activities during development, adulthood and aging (Limatola and Ransohoff, 2014), strongly suggest that the effects of CX_3CR1 ablation observed in the RTT model in large part came from blockage of neuron–microglia interaction.

Microglia processes make brief and direct contacts with synapses with regular frequencies, which depend on neuronal activity and glutamate level in the microenvironment (Wake et al., 2009; Li et al., 2012). Microglia thus perform delicate regulation of neuronal activity, using glutamate as an essential signaling molecule. Interestingly, the net consequence of microglia-neuron contact enhanced by activity-dependent glutamate release is reduced neuronal activity (Li et al., 2012). Our previous *in vitro* and *in vivo* data showed that microglia in *Mecp2KO* mice substantially over-produce glutamate and reactive oxygen species (ROS) due to aberrant expressions of bioenergetics genes regulated by MeCP2 (Maezawa and Jin, 2010; Jin et al., 2015). Therefore it is conceivable that blocking neuron–microglia interaction by CX_3CR1 ablation in RTT mice would ameliorate microglial suppression of neuronal activity from disrupted glutamate homeostasis, and dampen the potential synaptotoxicity inflicted by high levels of focal glutamate and ROS. Our data is consistent with this notion. Interestingly, CX_3CR1 ablation also restored the microglial morphology to the WT levels in several anatomic regions. It remains to be determined if CX_3CR1 ablation improves microglial function and morphology via a cell-autonomous mechanism or by blocking the detrimental non-cell autonomous influences from abnormal MeCP2-deficient neurons. The other interesting and perhaps somewhat surprising finding is that complete (*Cx3cr*$^{-/-}$) and partial (*Cx3cr1*$^{-/+}$) ablation of CX_3CR1 nearly equally

attenuated disease severity. This lack of a gene dosage dependent effect may suggest that the protective effect achieved by blocking neuron–microglia interaction is plateaued by ablating around half of the CX_3CR1. Further studies are required to fully address this question.

The other mechanism revealed for the beneficial effects of CX_3CR1 ablation is the enhanced neurotrophic action of microglia producing higher amount of IGF1, as evidenced by increases in both transcript and protein levels of IGF1 in *Mecp2KO–Cx3cr1*$^{-/-}$ and *Mecp2KO–Cx3cr1*$^{-/+}$ mice. Interestingly, the effects of CX_3CR1 ablation seem comparable to a previously conducted replacement therapy with recombinant human IGF1 (Castro et al., 2014). As shown in Fig. 7, we measured both total and free IGF1 levels based on the consideration that the free IGF1 level, representing molecules not bound to the carrier IGF binding proteins (IGFBPs), was considered by some authors the bioavailable form (Yee et al., 1994; Ueno et al., 2013). Although both *Mecp2KO–Cx3cr1*$^{-/+}$ and *Mecp2KO–Cx3cr1*$^{-/-}$ mice showed substantial increases in total IGF1 compared to *Mecp2KO* mice, the lack of significant difference in the level of free IGF1 between *Mecp2KO* and *Mecp2KO–Cx3cr1*$^{-/+}$ mice does not explain the comparable beneficial effects of heterozygous and homozygous *Cx3cr1* knockout (Fig. 7C). However, recent evidence indicates more complex regulations of IGF1 signaling by IGFBPs in which IGF1 signaling is either enhanced or atten uated depending on cellular context and microenvironment and suggests that total-IGF1 level is a more reliable index for the overall bioavailability of IGF1 rather than free IGF1 (Baxter, 2014).

The reported disease rectifying effect of providing *Mecp2KO* mice with WT myeloid cells by bone marrow transplantation is more robust than the effect we observed by CX_3CR1 ablation (Derecki et al., 2012), indicating that our approach only rectifies a portion of microglial/myeloid cell abnormalities in *Mecp2KO* mice. In addition to providing adequate amount of neurotrophic support by IGF1 and eliminating neurotoxic neuron–microglia interaction, another apparent advantage of providing *Mecp2KO* mice with WT myeloid is the restoration of phagocytotic activity, as the disease rectifying effects were diminished when phagocytotic activity was inhibited pharmacologically (Derecki et al., 2012).

Previous studies using the CX_3CR1 ablation approach were mainly conducted in models of adult brain disorders with a clear component of neuroinflammation such as Alzheimer's disease, Parkinson's disease, stroke, and multiple sclerosis. It was found that CX_3CL1–CX_3CR1 signaling is neuroprotective in some settings, but in other settings is required for neurotoxicity mediated by microglia (Sheridan and Murphy, 2013; Limatola and Ransohoff, 2014). Thus, the pathological significance of CX_3CR1-mediated neuron–microglia interaction depends on specific disease mechanisms and could be fundamentally different in pathological settings of developing brain. Recent reports revealed that CX_3CR1 is required for certain physiological neurodevelopmental processes such as synaptic pruning, neuronal survival, and glutamatergic synapse maturation (Limatola and Ransohoff, 2014). In contrast, in the *Mecp2KO* environment, the presence of CX_3CR1 is apparently detrimental to the neurodevelopmental trajectory. Our data, therefore, expand the neurodevelopmental role of neuron–microglia interaction to a more complex, context-dependent manner. To our knowledge, our report is the first to address the significance of CX_3CL1–CX_3CR1 signaling in a childhood neurodevelopmental disorder devoid of a clear component of

neuroinflammation, and suggests a novel therapeutic approach for RTT by targeting CX_3CR1 with specific antagonists or genetic downregulation. Various "anti-CX_3CR1" approaches, such as neutralizing antibodies against CX_3-CR1, small molecule and peptide inhibitors, and CX_3CR1 siRNA, have been tested in models of other disorders and could have potential therapeutic utilities for RTT (Kiyomoto et al., 2013; Poupel et al., 2013; Wu et al., 2013; Ridderstad Wollberg et al., 2014). Moreover, RTT is highly relevant to our understanding of autism, a group of high-prevalence developmental disorders. RTT is one of few autistic diseases whose cause is identified as a single gene mutation and shares important pathogenic pathways with autism (Amir et al., 1999; Zoghbi, 2003; Levitt and Campbell, 2009; Chao et al., 2010; Gonzales, 2010). MeCP2 is also deficient in a large subgroup of autistic individuals (Samaco et al., 2005; Moretti and Zoghbi, 2006; Nagarajan et al., 2008; Levitt and Campbell, 2009; Ramocki et al., 2009). Therefore, our results may also implicate novel mechanisms and therapeutic approaches for autism where microglia dysfunction could also play a role (Maezawa et al., 2011; Schafer et al., 2013; Bilimoria and Stevens, 2015).

Acknowledgments

This work was supported by the US National Institute of Health (HD073631, HD064817, and HD079125) and the University of California, Davis. We thank Dr. Danielle Harvey at UC Davis Department of Public Health for assistance in statistics analysis. The authors declare no competing financial interests.

References

Abdala AP, Dutschmann M, Bissonnette JM, Paton JF. Correction of respiratory disorders in a mouse model of Rett syndrome. Proc Natl Acad Sci U SA. 2010; 107:18208–18213.

Alvarez-Saavedra M, Saez MA, Kang D, Zoghbi HY, Young JI. Cell-specific expression of wild-type MeCP2 in mouse models of Rett syndrome yields insight about pathogenesis. Human Mol Genet. 2007; 16:2315–2325. [PubMed: 17635839]

Amir RE, Van den Veyver IB, Wan M, Tran CQ, Francke U, Zoghbi HY. Rett syndrome is caused by mutations in X-linked MECP2, encoding methyl-CpG-binding protein 2. Nat Genet. 1999; 23:185–188. [PubMed: 10508514]

Baxter RC. IGF binding proteins in cancer: mechanistic and clinical insights. Nat Rev Cancer. 2014; 14:329–341. [PubMed: 24722429]

Bilimoria PM, Stevens B. Microglia function during brain development: new insights from animal models. Brain Res. 2015; 1617:7–17. [PubMed: 25463024]

Cardona AE, Pioro EP, Sasse ME, Kostenko V, Cardona SM, Dijkstra IM, Huang D, Kidd G, Dombrowski S, Dutta R, Lee JC, Cook DN, Jung S, Lira SA, Littman DR, Ransohoff RM. Control of microglial neurotoxicity by the fractalkine receptor. Nature Neurosci. 2006; 9:917–924. [PubMed: 16732273]

Castro J, Garcia RI, Kwok S, Banerjee A, Petravicz J, Woodson J, Mellios N, Tropea D, Sur M. Functional recovery with recombinant human IGF1 treatment in a mouse model of Rett Syndrome. Proc Natl Acad Sci USA. 2014; 111:9941–9946. [PubMed: 24958891]

Chahrour M, Zoghbi HY. The story of Rett syndrome: from clinic to neurobiology. Neuron. 2007; 56:422–437. [PubMed: 17988628]

Chahrour M, Jung SY, Shaw C, Zhou X, Wong ST, Qin J, Zoghbi HY. MeCP2, a key contributor to neurological disease, activates and represses transcription. Science. 2008; 320:1224–1229. [PubMed: 18511691]

Chao HT, Chen H, Samaco RC, Xue M, Chahrour M, Yoo J, Neul JL, Gong S, Lu HC, Heintz N, Ekker M, Rubenstein JL, Noebels JL, Rosenmund C, Zoghbi HY. Dysfunction in GABA signalling

mediates autism-like stereotypies and Rett syndrome phenotypes. Nature. 2010; 468:263–269. [PubMed: 21068835]

Chen RZ, Akbarian S, Tudor M, Jaenisch R. Deficiency of methyl-CpG binding protein-2 in CNS neurons results in a Rett-like phenotype in mice. Nat Genet. 2001; 27:327–331. [PubMed: 11242118]

Collins SM, Surette M, Bercik P. The interplay between the intestinal microbiota and the brain. Nat Rev Microbiol. 2012; 10:735–742. [PubMed: 23000955]

Cronk JC, Derecki NC, Litvak V, Kipnis J. Unexpected cellular players in Rett syndrome pathology. Neurobiol Dis. 2015a

Cronk JC, Derecki NC, Ji E, Xu Y, Lampano AE, Smirnov I, Baker W, Norris GT, Marin I, Coddington N, Wolf Y, Turner SD, Aderem A, Klibanov AL, Harris TH, Jung S, Litvak V, Kipnis J. Methyl-CpG binding protein 2 regulates microglia and macrophage gene expression in response to inflammatory stimuli. Immunity. 2015b; 42:679–691. [PubMed: 25902482]

Deacon RMJ. Measuring motor coordination in mice. Jove J Vis Exp. 2013

Derecki NC, Cronk JC, Lu Z, Xu E, Abbott SB, Guyenet PG, Kipnis J. Wild-type microglia arrest pathology in a mouse model of Rett syndrome. Nature. 2012; 484:105–109. [PubMed: 22425995]

Derecki NC, Cronk JC, Kipnis J. The role of microglia in brain maintenance: implications for Rett syndrome. Trends Immunol. 2013; 34:144–150. [PubMed: 23122051]

Garg SK, Lioy DT, Cheval H, McGann JC, Bissonnette JM, Murtha MJ, Foust KD, Kaspar BK, Bird A, Mandel G. Systemic delivery of MeCP2 rescues behavioral and cellular deficits in female mouse models of rett syndrome. J Neurosci. 2013; 33:13612–13620. [PubMed: 23966684]

Gonzales ML, LaSalle JM. The role of MeCP2 in brain development and neurodevelopmental disorders. Current Psychiatry Reports. 2010

Guy J, Hendrich B, Holmes M, Martin JE, Bird A. A mouse Mecp2-null mutation causes neurological symptoms that mimic Rett syndrome. Nat Genet. 2001; 27:322–326. [PubMed: 11242117]

Guy J, Gan J, Selfridge J, Cobb S, Bird A. Reversal of neurological defects in a mouse model of Rett syndrome. Science. 2007; 315:1143–1147. [PubMed: 17289941]

Harrison JK, Jiang Y, Chen SZ, Xia YY, Maciejewski D, McNamara RK, Streit WJ, Salafranca MN, Adhikari S, Thompson DA, Botti P, Bacon KB, Feng LL. Role for neuronally derived fractalkine in mediating interactions between neurons and CX3CR1-expressing microglia. Proc Natl Acad Sci USA. 1998; 95:10896–10901. [PubMed: 9724801]

Jin LW, Horiuchi M, Wulff H, Liu XB, Cortopassi GA, Erickson JD, Maezawa I. Dysregulation of glutamine transporter SNAT1 in Rett syndrome microglia: a mechanism for mitochondrial dysfunction and neurotoxicity. J Neurosci. 2015; 35:2516–2529. [PubMed: 25673846]

Katz DM, Dutschmann M, Ramirez JM, Hilaire G. Breathing disorders in Rett syndrome: progressive neurochemical dysfunction in the respiratory network after birth. Respir Physiol Neurobiol. 2009; 168:101–108. [PubMed: 19394452]

Khroyan TV, Zhang JX, Yang LY, Zou BD, Xie J, Pascual C, Malik A, Xie JL, Zaveri NT, Vazquez J, Polgar W, Toll L, Fang JD, Xie XM. Rodent motor and neuropsychological behaviour measured in home cages using the integrated modular platform SmartCage (TM). Clin Exp Pharmacol Physiol. 2012; 39:614–622. [PubMed: 22540540]

Kiyomoto M, Shinoda M, Okada-Ogawa A, Noma N, Shibuta K, Tsuboi Y, Sessle BJ, Imamura Y, Iwata K. Fractalkine signaling in microglia contributes to ectopic orofacial pain following trapezius muscle inflammation. J Neurosci. 2013; 33:7667–7680. [PubMed: 23637160]

Levitt P, Campbell DB. The genetic and neurobiologic compass points toward common signaling dysfunctions in autism spectrum disorders. J Clin Invest. 2009; 119:747–754. [PubMed: 19339766]

Li Y, Du XF, Liu CS, Wen ZL, Du JL. Reciprocal regulation between resting microglial dynamics and neuronal activity in vivo. Dev Cell. 2012; 23:1189– 1202. [PubMed: 23201120]

Limatola C, Ransohoff RM. Modulating neurotoxicity through CX_3CL1/CX_3CR1 signaling. Front Cell Neurosci. 2014; 8

Lioy DT, Garg SK, Monaghan CE, Raber J, Foust KD, Kaspar BK, Hirrlinger PG, Kirchhoff F, Bissonnette JM, Ballas N, Mandel G. A role for glia in the progression of Rett's syndrome. Nature. 2011; 475:497–500. [PubMed: 21716289]

Livak KJ, Schmittgen TD. Analysis of relative gene expression data using real-time quantitative PCR and the 2(T)(−Delta Delta C) method. Methods. 2001; 25:402–408. [PubMed: 11846609]

Maezawa I, Jin LW. Rett syndrome microglia damage dendrites and synapses by the elevated release of glutamate. J Neurosci. 2010; 30:5346–5356. [PubMed: 20392956]

Maezawa I, Calafiore M, Wulff H, Jin LW. Does microglial dysfunction play a role in autism and Rett syndrome? Neuron Glia Biol. 2011; 7:85–97. [PubMed: 22717189]

Moretti P, Zoghbi HY. MeCP2 dysfunction in Rett syndrome and related disorders. Curr Opin Genet Dev. 2006; 16:276–281. [PubMed: 16647848]

Nagarajan RP, Patzel KA, Martin M, Yasui DH, Swanberg SE, Hertz-Picciotto I, Hansen RL, Van de Water J, Pessah IN, Jiang R, Robinson WP, LaSalle JM. MECP2 promoter methylation and X chromosome inactivation in autism. Autism Res. 2008; 1:169–178. [PubMed: 19132145]

Niess JH, Brand S, Gu X, Landsman L, Jung S, McCormick BA, Vyas JM, Boes M, Ploegh HL, Fox JG, Littman DR, Reinecker HC. CX3CR1-mediated dendritic cell access to the intestinal lumen and bacterial clearance. Science. 2005; 307:254–258. [PubMed: 15653504]

Poupel L, Boissonnas A, Hermand P, Dorgham K, Guyon E, Auvynet C, Charles FS, Lesnik P, Deterre P, Combadiere C. Pharmacological inhibition of the chemokine receptor, CX3CR1, reduces atherosclerosis in mice. Arteriosclerosis Thrombosis Vasc Biol. 2013; 33:2297–2305.

Ramocki MB, Peters SU, Tavyev YJ, Zhang F, Carvalho CM, Schaaf CP, Richman R, Fang P, Glaze DG, Lupski JR, Zoghbi HY. Autism and other neuropsychiatric symptoms are prevalent in individuals with MeCP2 duplication syndrome. Ann Neurol. 2009; 66:771–782. [PubMed: 20035514]

Ridderstad Wollberg A, Ericsson-Dahlstrand A, Jureus A, Ekerot P, Simon S, Nilsson M, Wiklund SJ, Berg AL, Ferm M, Sunnemark D, Johansson R. Pharmacological inhibition of the chemokine receptor CX3CR1 attenuates disease in a chronic-relapsing rat model for multiple sclerosis. Proc Natl Acad Sci USA. 2014; 111:5409–5414. [PubMed: 24706865]

Robinson L, Guy J, McKay L, Brockett E, Spike RC, Selfridge J, De Sousa D, Merusi C, Riedel G, Bird A, Cobb SR. Morphological and functional reversal of phenotypes in a mouse model of Rett syndrome. Brain. 2012; 135:2699– 2710. [PubMed: 22525157]

Samaco RC, Hogart A, LaSalle JM. Epigenetic overlap in autism-spectrum neurodevelopmental disorders: MECP2 deficiency causes reduced expression of UBE3A and GABRB3. Human Mol Genet. 2005; 14:483–492. [PubMed: 15615769]

Schafer DP, Lehrman EK, Stevens B. The “quad-partite” synapse: microglia-synapse interactions in the developing and mature CNS. Glia. 2013; 61:24–36. [PubMed: 22829357]

Sheridan GK, Murphy KJ. Neuron-glia crosstalk in health and disease: fractalkine and CX3CR1 take centre stage. Open Biol. 2013; 3:130181. [PubMed: 24352739]

Stearns NA, Schaevitz LR, Bowling H, Nag N, Berger UV, Berger-Sweeney J. Behavioral and anatomical abnormalities in Mecp2 mutant mice: a model for Rett syndrome. Neuroscience. 2007; 146:907–921. [PubMed: 17383101]

Ueno M, Fujita Y, Tanaka T, Nakamura Y, Kikuta J, Ishii M, Yamashita T. Layer V cortical neurons require microglial support for survival during postnatal development. Nature Neurosci. 2013; 16:543–551. [PubMed: 23525041]

Viemari JC, Roux JC, Tryba AK, Saywell V, Burnet H, Pena F, Zanella S, Bevengut M, Barthelemy-Requin M, Herzing LB, Moncla A, Mancini J, Ramirez JM, Villard L, Hilaire G. Mecp2 deficiency disrupts norepinephrine and respiratory systems in mice. J Neurosci. 2005; 25:11521–11530. [PubMed: 16354910]

Voituron N, Hilaire G. The benzodiazepine Midazolam mitigates the breathing defects of Mecp2-deficient mice. Respir Physiol Neurobiol. 2011; 177:56–60. [PubMed: 21315849]

Vrinten DH, Hamers FFT. ‘CatWalk’ automated quantitative gait analysis as a novel method to assess mechanical allodynia in the rat; a comparison with von Frey testing. Pain. 2003; 102:203–209. [PubMed: 12620612]

Wake H, Moorhouse AJ, Jinno S, Kohsaka S, Nabekura J. Resting microglia directly monitor the functional state of synapses in vivo and determine the fate of ischemic terminals. J Neurosci. 2009; 29:3974–3980. [PubMed: 19339593]

Wang J, et al. Wild-type microglia do not reverse pathology in mouse models of Rett syndrome. Nature. 2015; 521:E1–4. [PubMed: 25993969]

Wu J, Bie B, Yang H, Xu JJ, Brown DL, Naguib M. Suppression of central chemokine fractalkine receptor signaling alleviates amyloid-induced memory deficiency. Neurobiol Aging. 2013; 34:2843–2852. [PubMed: 23855980]

Yee D, Jackson JG, Kozelsky TW, Figueroa JA. Insulin-like growth-factor binding protein-1 expression inhibits insulin-like growth factor-I action in Mcf-7 breast–cancer cells. Cell Growth Differ. 1994; 5:73–77. [PubMed: 7510125]

Zanella S, Mebarek S, Lajard AM, Picard N, Dutschniann M, Hilaire G. Oral treatment with desipramine improves breathing and life span in Rett syndrome mouse model. Respir Physiol Neurobiol. 2008; 160:116–121. [PubMed: 17905670]

Zhan Y, Paolicelli RC, Sforazzini F, Weinhard L, Bolasco G, Pagani F, Vyssotski AL, Bifone A, Gozzi A, Ragozzino D, Gross CT. Deficient neuron–microglia signaling results in impaired functional brain connectivity and social behavior. Nature Neurosci. 2014; 17:400–406. [PubMed: 24487234]

Zoghbi HY. Postnatal neurodevelopmental disorders: meeting at the synapse? Science. 2003; 302:826–830. [PubMed: 14593168]

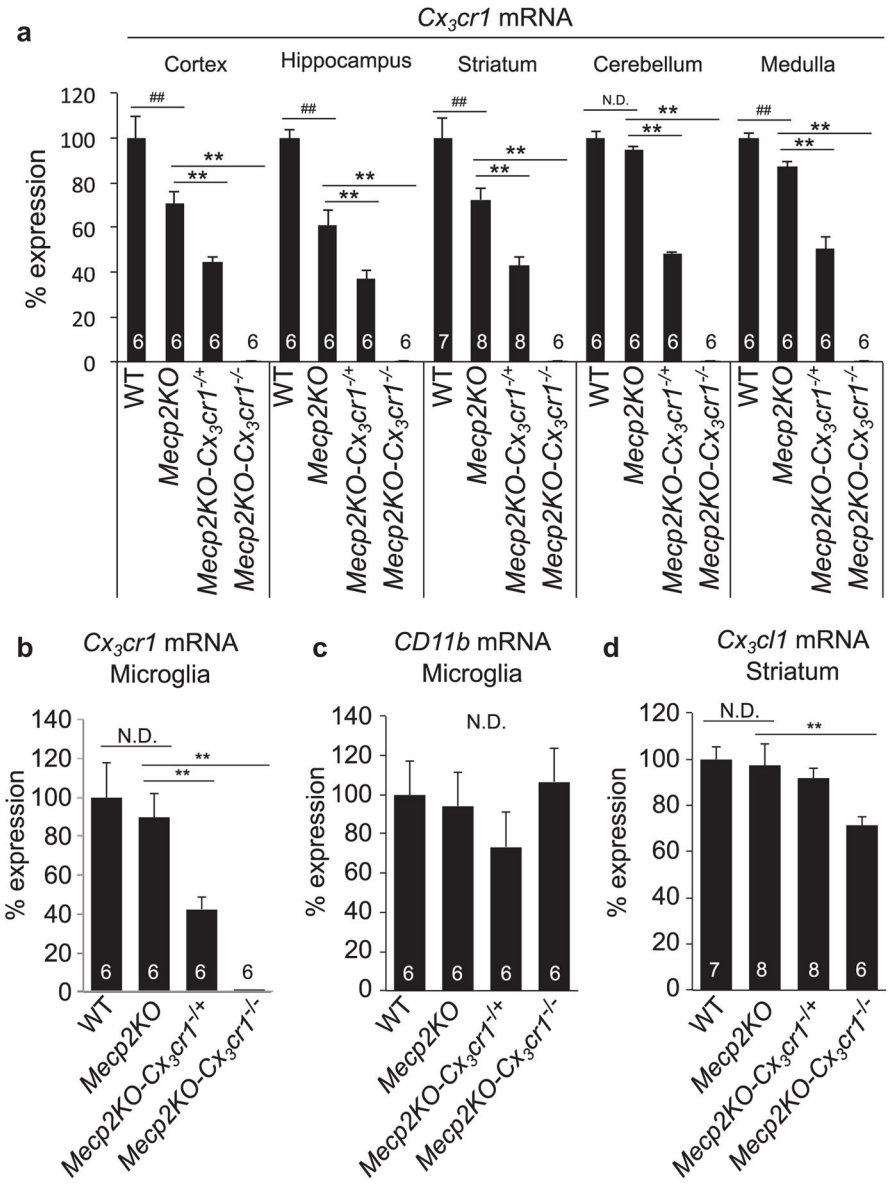

Fig. 1.

CX_3CR1 ablation in *Mecp2KO* mice. (**a**) qPCR quantification of *Cx3cr1* transcript in the cortex, the hippocampus, the striatum, the cerebellum, and the medulla from 8-week old mice of indicated genotype. (**b** and **c**) qPCR quantification of *Cx3cr1* and *Cd11b* transcript in microglia acutely isolated from 8-week old mice of indicated genotype. (**c**) qPCR quantification of *Cx3cl1* transcript in the striatum of 8-week old mice of indicated genotype. Sample size is indicated in each column. ## indicates $p < 0.01$ between WT and *Mecp2KO* mice. ** indicates $p < 0.01$ between *Mecp2KO* and *Mecp2KO–Cx3cr1*$^{-/+}$ or *Mecp2KO–Cx3cr1*$^{-/-}$. N.D. indicates "No difference" between the indicated groups.

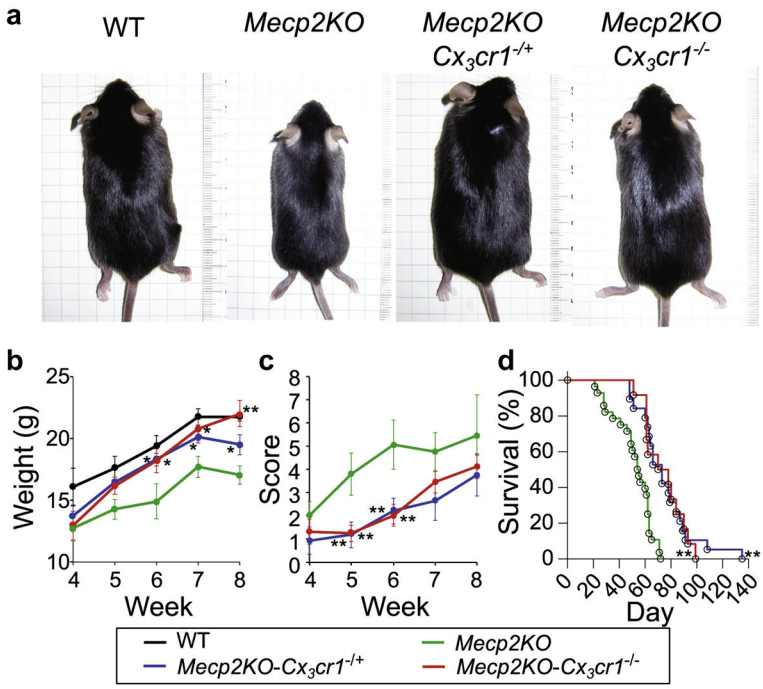

Fig. 2.

CX_3CR1 ablation improves the body weight and symptomatic score of *Mecp2KO* mice. In all figures, * indicates $p < 0.05$ and ** indicates $p < 0.01$, respectively. (**a**) Representative images of mice at 8 weeks of age. (**b**) Body weight and (**c**) symptomatic score of *Mecp2KO–Cx3cr1*$^{-/+}$ ($n = 18$), *Mecp2KO–Cx3cr1*$^{-/-}$ ($n = 8$), *Mecp2KO* ($n = 12$), and WT mice ($n = 9$). (**d**) Kaplan-Meier survival plot of *Mecp2KO–Cx3cr1*$^{-/+}$ ($n = 19$, mean ± SEM of average survival = 75 ± 5 days), *Mecp2KO–Cx3cr1*$^{-/-}$ ($n = 12$, 74 ± 4 days), and *Mecp2KO* ($n = 28$, 51 ± 3 days) mice.

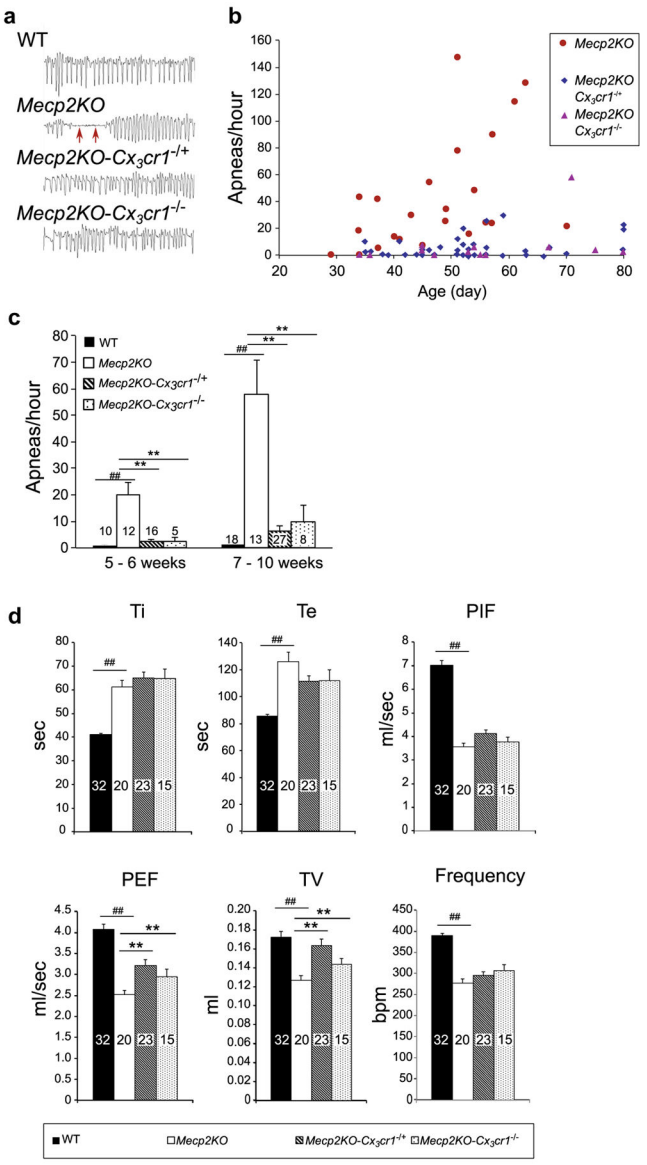

Fig. 3.

CX_3CR1 ablation improves the respiratory parameters of *Mecp2KO* mice. (**a**) Representative tracings of mice of indicated genotype at 8 weeks of age. The two red arrows point to an episode of apnea typically observed in *Mecp2KO* mice. (**b**) Apnea count was plotted as a function of age. *Mecp2KO–Cx3cr1*$^{-/+}$ and *Mecp2KO–Cx3cr1*$^{-/-}$ mice did not show increased apnea even after their median survival times (73 and 74 days, respectively), whereas *Mecp2KO* mice showed an age-dependent increase in apnea. (**c**) Number of apnea detected in mice of indicated genotype at 5–6 weeks and 7–10 weeks of age. (**d**) Respiratory parameters of 5,000 consecutive respiratory cycles from each recording were analyzed. *Mecp2KO* mice showed significantly prolonged inspiratory time (Ti) and expiratory time (Te), and significantly reduced peak inspiratory flow (PIF), peak expiratory flow (PEF), tidal ventilation (TV), and respiratory frequency compared to WT mice. This result indicates that both inspiration and expiration were impaired in *Mecp2*KO mice. The reduced PEF and TV

were significantly improved in *Mecp2KO–Cx3cr1*$^{-/+}$ and *Mecp2KO–Cx3cr1*$^{-/-}$ mice. ## indicates $p < 0.01$ between WT and *Mecp2KO* mice. ** indicates $p < 0.01$ between *Mecp2KO* and *Mecp2KO–Cx3cr1*$^{-/+}$ or *Mecp2KO–Cx3cr1*$^{-/-}$. The group size is indicated in the corresponding column.

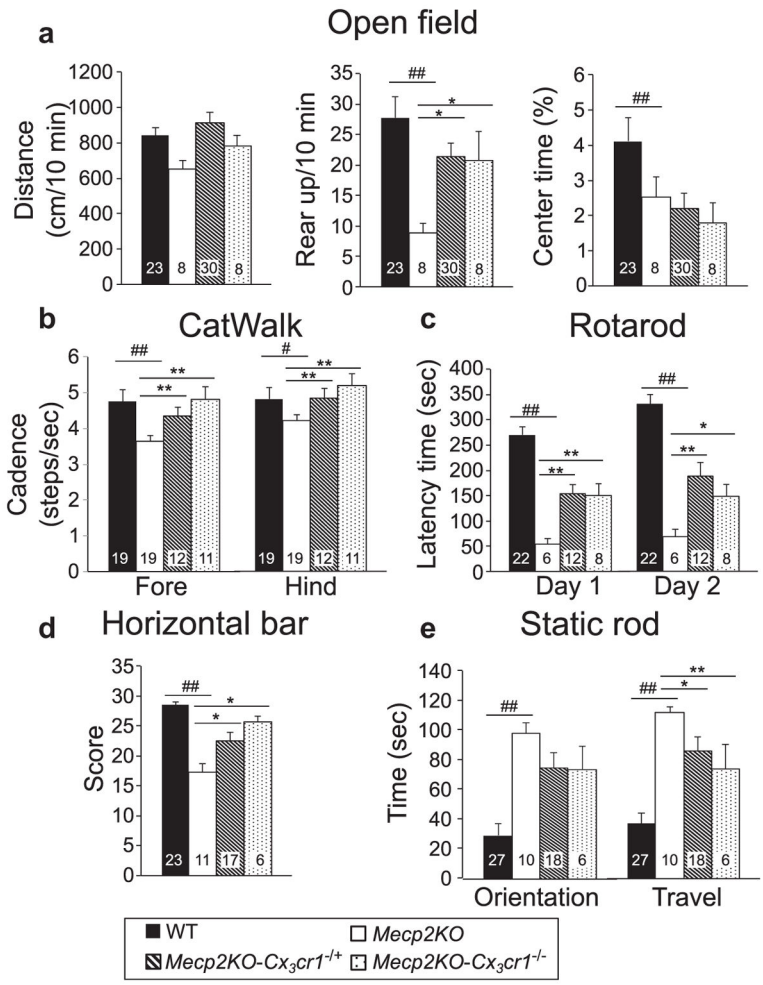

Fig. 4.

CX_3CR1 ablation improves the motor coordination and performance of *Mecp2KO* mice. (**a**) Travel distance (left), rear-up number (center) and center time (right) revealed in the open-field test; (**b**) cadence in the CatWalk gait analysis; (**c**) the latency time to fall in the Rotarod test; (**d**) horizontal bar test; and (**e**) static rod test of mice at 5–6 weeks of age. # and ## indicate $p < 0.05$ and $p < 0.01$, respectively, between WT and *Mecp2KO* mice. * and ** indicate $p < 0.05$ and $p < 0.01$, respectively, between *Mecp2KO* and *Mecp2KO–Cx3cr1*$^{-/+}$ or *Mecp2KO–Cx3cr1*$^{-/-}$. The group size is indicated in or above the corresponding column.

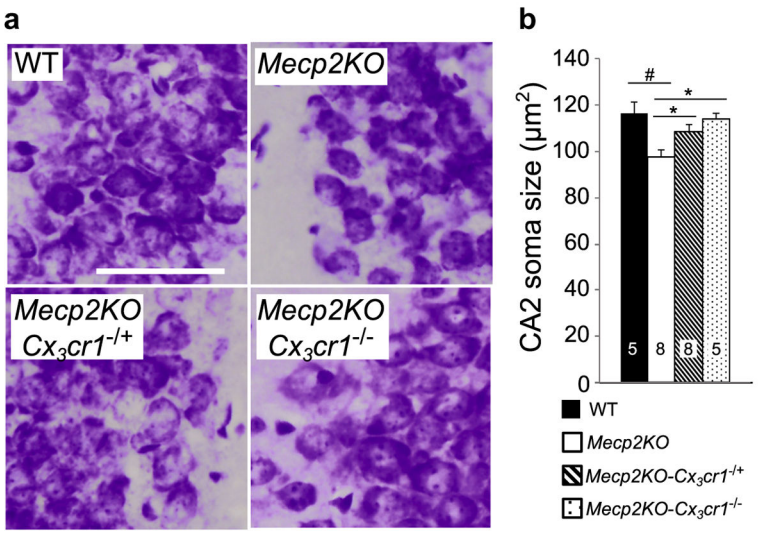

Fig. 5.

CX_3CR1 ablation recovers neuronal morphology in *Mecp2KO* mice. (**a**) Representative images of cresyl violet-stained neurons in hippocampal CA2 of 8-week-old mice of indicated genotype. Scale bar, 50 μm. (**b**) A quantitative comparison of soma size of CA2 neurons. # indicates $p < 0.05$ between WT and *Mecp2KO* mice. * indicates $p < 0.05$ between *Mecp2KO* and *Mecp2KO–Cx3cr1*$^{-/+}$ or *Mecp2KO–Cx3cr1*$^{-/-}$. The group size is indicated in the corresponding column.

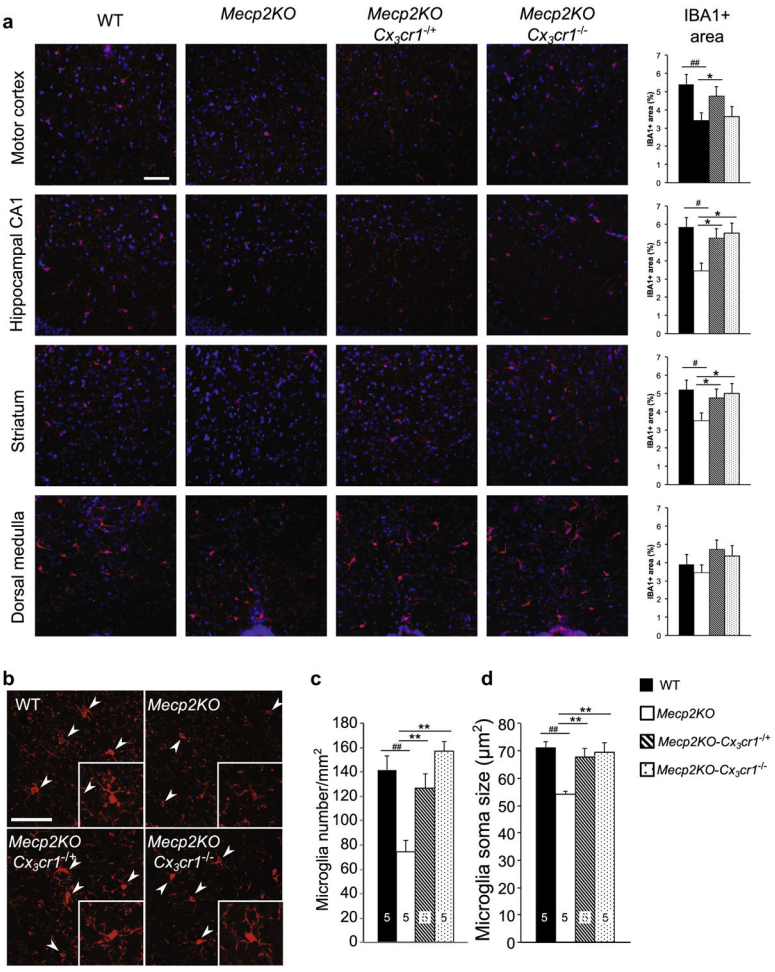

Fig. 6.

CX_3CR1 ablation recovers microglial morphology and abundancy in *Mecp2KO* mice. (**a**) Representative images of IBA1-immunoreactive microglia (red) with DAPI counterstain (blue) in the indicated anatomic regions of 8-week-old mice of indicated genotype. Scale bar, 50 μm. *Mecp2*KO mice showed less microglia with less apparent processes compared to *WT* mice in the motor cortex, hippocampal CA1, and striatum, but not in the medulla. These reductions were ameliorated by CX_3CR1 ablation. The bar graphs on the right present the corresponding quantification of IBA1-immunoreactive area in each brain region. (**b**) Representative images of anti-IBA1-stained microglia (red) in striatum. Arrowheads point to microglial soma. Scale bar, 50 μm. (**c** and **d**) Comparisons of microglial number (**c**) and microglial soma size (**d**) in the striatum. The group size is indicated in the corresponding column. $^{\#}$ and $^{\#\#}$ indicate $p < 0.05$ and $p < 0.01$, respectively, between WT and *Mecp2KO* mice. * and ** indicates $p < 0.05$ and $p < 0.01$, respectively, between *Mecp2KO* and *Mecp2KO–Cx3cr1*$^{-/+}$ or *Mecp2KO–Cx3cr1*$^{-/-}$. (For interpretation of the references to color in this figure legend, the reader is referred to the web version of this article.)

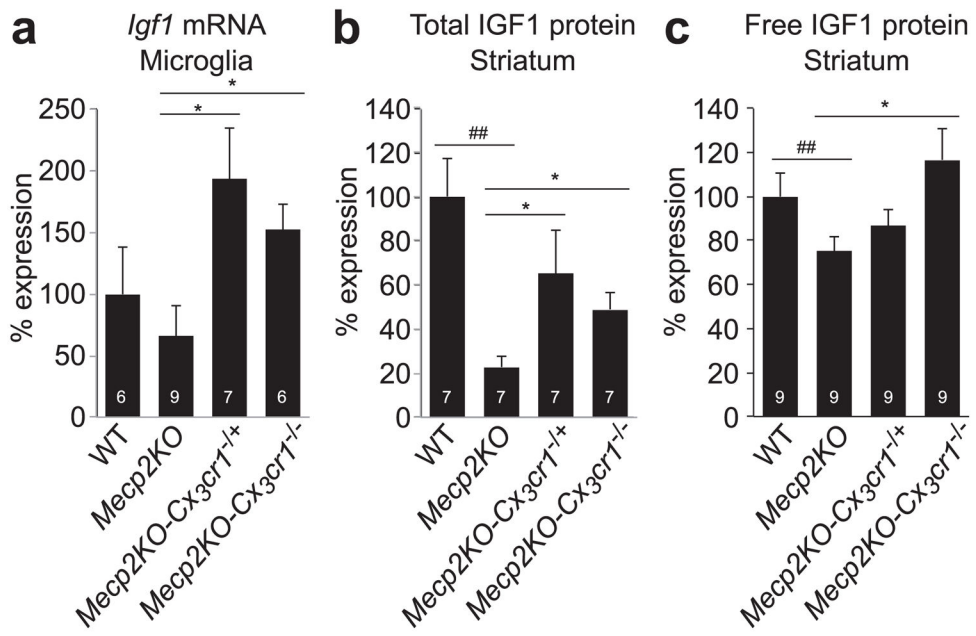

Fig. 7.

CX_3CR1 ablation increases the expression of IGF1 in *Mecp2KO* mice. (**a**) qPCR quantification of *Igf1* transcript in microglia acutely isolated from 8-week-old mice. *, $p < 0.05$ (**b** and **c**) ELISA quantification of total IGF1 (**b**) and free IGF1 (**c**) in striatum of 8-week-old mice. $^{\#\#}$ indicates $p < 0.01$ between WT and *Mecp2KO* mice. * and ** indicate $p < 0.05$ and $p < 0.01$, respectively, between *Mecp2KO* and *Mecp2KO–Cx3cr1*$^{-/+}$ or *Mecp2KO–Cx3cr1*$^{-/-}$. The group size is indicated in the corresponding column.